

¹ A Design for a Deep Underground Single-Phase
² Liquid Argon Time Projection Chamber for
³ Neutrino Physics and Astrophysics

⁴ March 12, 2015

Contents

2	1 Photon Detector	1
3	1.1 Introduction	1
4	1.2 Requirements and Goals	1
5	1.2.1 Beam-based physics	1
6	1.2.2 Proton decay and atmospheric physics	2
7	1.2.3 Low-energy physics	2
8	1.2.4 Required Performance	2
9	1.2.5 General Considerations	3
10	1.3 Photon Detector Prototype Designs	4
11	1.3.1 Cast or Bulk doped acrylic bars	4
12	1.3.2 Fiber-embedded bulk acrylic plate	6
13	1.3.3 LSU Photon detection panel production	7
14	1.3.4 Proof of concept and prototype detector results	9
15	1.3.5 R&D Work in progress and present Plans	10
16	1.3.6 Fiber bundle with WS-coated readiator	12
17	1.4 SiPM	14
18	1.5 Menchanical Support	14
19	1.6 Photon System Readout Electronics	18
20	1.6.1 Reference Design	18
21	1.6.2 Alternatives	23
22	1.7 Photon Detector Calibration	25
23	1.8 Installation	30

List of Figures

2	1.1	Probability of photon being detected in detectors when depositing energy	4
3	1.2	Schematic drawing of a light guide with its photosensors	5
4	1.3	LSU photon-detection panel	8
5	1.4	Light yield for the fiber LSU PD panels with alpha source in LAr	10
6	1.5	Summed charge plots of SiPMs in response to muon hodoscope trigger .	11
7	1.6	Fiber-bundle PD prototype (early one-sided version)	12
8	1.7	Full APA frame with ten photon detectors mounted inside the frame . .	15
9	1.8	Photograph of 40 cm long bar-based prototype mounted in test frame . .	16
10	1.9	Mechanical assembly drawing of frame system	17
11	1.10	Blow up of APA fram showing PD insertion location	17
12	1.11	Slot and rail showing mounting location of photon detector	18
13	1.12	Block diagram of the photon detector signal processing system	19
14	1.13	Picture of the SSP module	21
15	1.14	Block diagram the SSP module	22
16	1.15	Concept of the UV-light calibration system	27
17	1.16	Diagrams of diffusers, their locations and UV light transport	28
18	1.17	Photon detector calibration module (PDCM) layout	29
19	1.18	Simulated light distributions of the 35-ton APA, two cases	29

List of Tables

¹	1.1	Individual photon collection efficiencies	3
²	1.2	Light guide technologies	5
³	1.3	Physics requirements for the photon detector electronics	19

⁵ Todo list

⁶ (need general TPC cell map with better description)	4
⁷ Fuzzy at this size	5
¹ check ref	18
¹ check ref	18
² No fig1 exists for: Block diagram of the photon detector signal processing system.	19
³ fix	25

⁴ Chapter 1

⁵ Photon Detector

ch:photon

⁶ 1.1 Introduction

- ¹ Liquid argon is an excellent scintillating medium. With an average energy needed
- ² to produce a photon of 19.5 eV (at zero field) a typical particle depositing 1 MeV in
- ³ liquid argon will generate 40,000 photons with wavelength of 128 nm. At higher fields
- ⁴ this will be reduced but at 500 V/cm the yield is still about \sim 20,000 photons per
- ⁵ MeV. Roughly 1/3 of the photons are promptly emitted after about 6 ns while the
- ⁶ rest are emitted with a delay of 1100-1600 ns. LAr is highly transparent to the
- ⁷ 128 VUV photons with a Rayleigh scattering length and absorption length of 95 cm
- ⁸ and >200 cm respectively. The relatively large light yield makes the scintillation
- ⁹ process an excellent candidate for determination of t_0 for non-beam related events.
- ¹⁰ Detection of the scintillation light may also be helpful in background rejection.

¹¹ 1.2 Requirements and Goals

¹² 1.2.1 Beam-based physics

- ¹³ There are no requirements for the beam-based physics program, as the machine clock
- ¹⁴ will provide a t_0 with roughly 10 μ s resolution. Given that the electron drift is 1.6
- ¹⁵ mm/ μ s the uncertainty to the electron lifetime correction is small if the beam timing
- ¹⁶ is used. The photon system can be useful in determining the t_0 of cosmic ray events
- ¹⁷ and events from radiological decays as well as giving a handle to the location of beam
- ¹⁸ events in the LAr volume with respect to fiducial boundaries. The impact of the
- ¹⁹ LAr scintillation light on the detector performance needs to be determined, but it

20 is not expected that the reduction in backgrounds for the oscillation program will
21 introduce additional requirements to the photon system design.

22 **1.2.2 Proton decay and atmospheric physics**

1 The photon detector system must provide the t_0 for non-beam related physics chan-
2 nels if a correction for electron recombination during drift is to be applied. The
3 requirements for electronics and hadronic energy resolution for the proton decay and
4 the atmospheric neutrino program are $1\%/\sqrt{E(\text{GeV})} \oplus 1\%$ and $30\%/\sqrt{E(\text{GeV})}$ re-
5 spectively. With these resolutions the collected charge must be accurately corrected
6 for recombination. Therefore the photon system must provide a t_0 for particles with
7 >100 MeV with $>95\%$ efficiency in the fiducial volume of the detector.

8 **1.2.3 Low-energy physics**

9 Supernova events will produce neutrinos down to about ~ 5 MeV. Studies have es-
10 timated the momentum resolution for 5 MeV electrons to be 20% using only TPC
11 information and assuming a highly efficient trigger and an electron lifetime of 5 ms.
12 The impact of various detector resolutions on the physics potential of LBNE has not
13 been studied in detail. At present there is no strong requirement that the energy
14 resolution must be better than 20% so no requirement on the photon system trigger
15 efficiency is set at this time. However it is clear that if a detector design can be
16 found the energy resolution would greatly improve. A goal of the photon detection
17 R&D is to develop a system with the lowest possible threshold for a reasonable cost.
18 At time of the start of final design a final decision as to the configuration will need
19 to be made based on cost and added physics capability.

20 **1.2.4 Required Performance**

21 To achieve the physics goals in the previous section the performance of the photon
22 detection system must be understood. The prototype readout electronics described
23 in section 1.6 have been shown to detect the single p.e. signals associated with the
24 late scintillation light but future versions may sacrifice this ability to mitigate high
25 channel costs. It is assumed that the physics goals of the photon detection system
26 will be met using on the prompt scintillation light.

27 The performance, or overall photon collection efficiency, is given by the following,
28 where it is assumed only prompt light is collected:

$$\frac{N_{pe}}{MeV} = N_{128} \cdot \epsilon_{geom} \cdot \epsilon_E \cdot \epsilon_{mesh} \cdot \epsilon_{conv} \cdot \epsilon_{capt} \epsilon_{tran} \cdot \epsilon_{QE} \quad (1.1) \quad \boxed{\text{eff_eqn}}$$

29 The efficiencies leading to the overall number of photo-electrons collected by the
 30 photon detection system, $\frac{N_{pe}}{MeV}$, are given in table [Table-Eff](#).

Table 1.1: Individual photon collection efficiencies

Factor	Description	Value	Comments
ϵ_{geom}	geometric acceptance	0.0036	historical average
ϵ_E	field correction	0.6	500 V/cm
ϵ_{mesh}	TPC wire shadowing	.83 (30-150°)	^{HimmelMesh} falls off sharply [?]
ϵ_{conv}	TPB conversion	1	^{Lip:german} see ref. [?]
ϵ_{capt}	waveguide incident	0.5	about half converted photons
			travel into waveguide
ϵ_{tran}	waveguide transmission	TBD	prototype dependent
ϵ_{QE}	SiPM QE	.31	SensL b-series

31 Using equation 1.1 it is seen that to detect a 2 p.e. signal, likely to be dis-
 1 criminated from noise, the transport efficiency of 1.2%. Of course this value is very
 2 position dependent as the geometric acceptance, wire shadowing, and transport cor-
 3 rections all depend on the location of the event. Figure [fig:photon_map](#) 1.1 shows the probability of
 4 (?) MeV energy deposition neing detected in the photon detectors.

5 The TPC wire mesh shadowing is also quite location dependent as photon angles,
 6 relative to the wire plane, lead to rapid loss in transmission below 30° and greater
 7 than 150°. Lastly the photon detector paddles themselves can have position depen-
 8 dent response to incident photons due to the attenuation length of the waveguide.
 9 The photon detector simulation, which is nearing stable operation, will be able to
 10 better estimate the efficiencies coming from geometric acceptance correction.

11 1.2.5 General Considerations

12 In the event that higher photon collection efficiencies can be achieved it should be
 13 possible to improve the energy resolution of the detector by adding the photon yield
 14 to the electron yield information. However this requires several orders of improve-
 15 ment in light collection efficiency so it is beyond the scope of present designed.

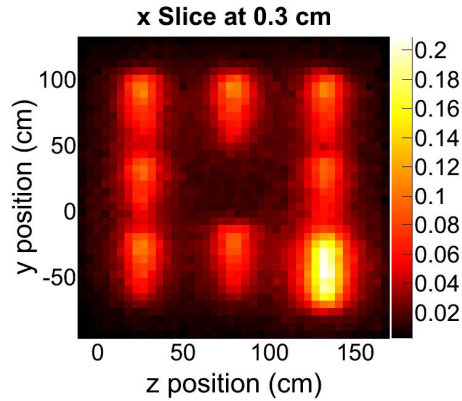


Figure 1.1: Photon map giving the probability of photon being detected in the photon detectors when depositing energy at map location.

(need general TPC cell map with better description)

`fig:photon_map`

1.3 Photon Detector Prototype Designs

All design considered for the photon detector have been based on the use of wavelength-shifting coating, or bulk doping, of plastic materials coupled to silicon photomultipliers (SiPMs). The reference design 1.3.1 utilizes a coated acrylic waveguide coupled to SiPMs. Alternataate designs, described in the following section, have been developed to optimize coverage, cost, and attenuation length.

1.3.1 Cast or Bulk doped acrylic bars

The reference design for the photon detection system is based on light guides that are coated with wavelength shifter. The 128 nm scintillation photons from liquid argon interact with the wavelength shifter on the light guide surface and 430 nm light is re-emitted in the bar. The light guide channels the light to photodetectors at its end.

A schematic drawing of a light guide with its photosensors is shown in Figure 1.2.

The prototype light guides are bars with a footprint $2.54\text{ cm} \times 0.6\text{ cm}$. The concept is described in Ref. [?].

The wavelength shifter converts VUV scintillation photons striking it to 430 nm photons inside the bar, with an efficiency of $\sim 50\%$ of converting a VUV to an optical photon [?]. A fraction of the waveshifted optical photons are internally reflected to the bar's end where they are detected by SiPMs whose QE is well matched to the

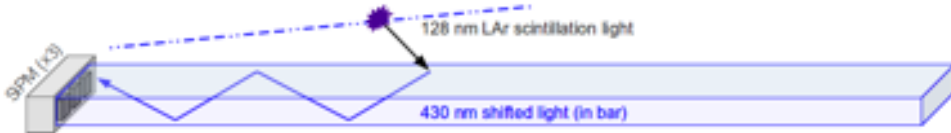


Figure 1.2: Schematic drawing of a light guide with its photosensors. The bars have embedded wavelength shifter (WLS), either TPB or bis-MSB. Three SiPMs collect the waveshifted photons that have been internally reflected to the bar's end.

Fuzzy at this size

fig:WaveguideS

¹⁷ 430 nm waveshifted photons. The light guides were made with one of two wavelength shifters: the conventional TPB (1,1,4,4-tetraphenyl-1,3-butadiene) and the ¹⁹ less expensive alternative bis-MSB (1,4-bis-(o-methyl-styryl)-benzene). Preliminary ¹ studies with a VUV monochromator show that the two wavelength shifters compare ^{bib:baptistaJINST} ² favorably in their waveshifting efficiency ^[?]. A testing program is currently underway ³ to compare their relative performance in liquid argon.

⁴ The prototype light guides being studied at Indiana are made with different three ^{tab:lightGuides} ⁵ technologies. These technologies are listed in Table 1.2.

Table 1.2: Light guide technologies

Label	Light Guide Technologies
(a)	clear acrylic, dip-coated
(b)	doped Eljen PVT light guide, dip-coated
(c)	doped Eljen polystyrene light guide, dip-coated

⁶ (a) The clear acrylic bars are made from blanks of commercially available Lucite-⁷ UTRAN cast UVT acrylic sheet that has been laser-cut and diamond-polished into ⁸ bars of the proper size. Lucite-UTRAN has the longest attenuation length of the ⁹ acrylics tested ^[?]. The Eljen¹ bars are commercial light guides that are doped with ¹⁰ J2 green fluor (equivalent to Y11). Two types of light guides were purchased from ¹¹ Eljen. (b) The light guides were fabricated from polyvinyl toluene (PVT). These are ¹² the standard Eljen product EJ-280. The quantum efficiency of the fluorescent dopant ¹³ in EJ-280 is 0.86, so the second shift in wavelength does not markedly degrade the ¹⁴ photon detector efficiency. (c) The light guides were fabricated from polystyrene. ¹⁵ These light guides were ordered because PVT bars can craze if cooled too rapidly.

¹<http://www.eljentechnology.com>

16 Although the PVT light guides may be brighter, no instance of crazing has ever been
17 observed in polystyrene light guides.

18 For the acrylic light guides, the WLS must be embedded in the plastic at the bar's
1 surface so that 128 nm scintillation photons can generate optical 430 nm photons
2 within the volume of the plastic. Otherwise the VUV photons will not be trapped
3 by the light guide. For the Eljen bars, the wavelength shifter can either be embed-
4 ded in the plastic as with the acrylic. Or it can be deposited on a plate or film
5 placed in proximity to the light guides. The J2 wavelength shifter then converts the
6 resulting 430 nm photons inside the light guides where they are channeled to the
7 photodetectors.

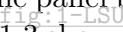
8 To embed the WLS at the surface of the light guides, a "dip-coating" process
9 was developed at Indiana University. Before the WLS was applied to the acrylic
10 bars, they were annealed at 80°C for one hour. The Eljen bars were not annealed.
11 The WLS was dissolved in the organic solvent dichlormethane (CH_2Cl_2). For these
12 waveguides there were 5 gm of wavelength shifter dissolved in 1,000 gm of DCM. A
13 series of experiments showed that this concentration was optimum. A bar was first
14 dipped into the WLS mixture for 15 seconds and then removed. It was then hung
15 in the dark for at least two hours to dry. Once dry, the ends of the bars were flycut.
16 Currently designs are being fabricated that put an acrylic plate painted with WLS
17 or a thin film impregnated with WLS in front of the Eljen light guides .

18 In summer 2015 these designs will all be tested side-by-side at the TallBo dewar
19 facility at Fermilab under uniform, low-contamination conditions. In addition to
20 the designs described above, these tests will include photon detector designs from
21 Colorado State University and Louisiana State University. This experiment will
22 compare the relative performance and the absolute efficiency for all designs scaled
23 to 1.5 m.

24 **1.3.2 Fiber-embedded bulk acrylic plate**

25 At LSU, Thomas Kutter and team have developed a VUV photon detector design for
26 a large LAr detector that overcomes some of the shortcomings of the present LBNE
27 baseline photon detectors. The LSU photon detector design allows for a very large
28 area coverage thereby increasing the geometrical acceptance of the photon detectors.
29 The number of required SiPMs and readout channels per unit detector area covered
30 with photon detection panels has been significantly reduced to keep the overall cost
31 for the photon detection system at or below the present design while increasing the
32 geometrical acceptance at the same time.

33 The photon detection system consists of a TPB coated acrylic panel with an

34 embedded S-shaped wavelength shifting (WLS) fiber. The fiber is read out by two
35 SiPMs, which are coupled to either end of the fiber and serves to transport the
36 light over long distances with minimal attenuation. The double-ended fiber readout
1 has the added benefit to provide some position dependence to the light generation
2 along the panel by comparing relative signal sizes and arrival times in the two SiPMs.
3  Figure 1.3 show a drawing of the layout and a picture of a prototype photon detection
4 panel in the test stand at LSU. The incoming 128nm VUV Ar scintillation light
5 will be converted by the thin TPB layer on the acrylic panel and re-emitted with
6 wavelength peaking at 430nm in an isotropic way. About 50% of the light would be
7 emitted into the acrylic panel where some fraction will be absorbed by the WLS fiber
8 and converted to light with a peak intensity of about 480 - 500 nm. The green light
9 exiting the fiber is well matched to the peak photon detection efficiency of typical
10 SiPMs.

11 **1.3.3 LSU Photon detection panel production**

12 The photon detection panels are produced from 0.25 thick sheet UVT acrylic and
13 cut to size. For a first series of prototypes the acrylic panel dimensions were chosen
14 to closely match the area of 4 bars of the LBNE baseline photon detection system.
15 The groove is cut with a CNC mill in several passes to achieve good groove surface
16 quality, which is important for good light transmission from the bulk acrylic to the
17 fiber. The panels are dip coated with TPB and left to dry prior to insertion of the
18 WLS fiber. Panels with two and three layers of fibers inserted and glued into the
19 groove have been produced. Fiber ends are cut and polished. The resulting acrylic
20 panels are then inserted into a custom made mechanical frame which was designed
21 by David Warner at CSU. The end caps of the mechanical frame house one SiPM
22 on either end. The presently used 6x6 mm² active area SiPM are spring mounted
23 to ensure good contact between the active area and the fiber ends. The leads of
24 the SiPMs are connected to a small PCB onto which 2m long twisted pair coax
25 cables are soldered to supply the SiPM with a bias voltage and read out signals. The
26 other cable ends are typically connected to pre-amplifiers before leading to a DAQ
27 system. Components for the photon detection panels are inspected at all stages of
28 the manufacturing process for quality. Due to the small number of panels produced
29 to date no quantitative quality control parameters have been defined yet. Proper
30 connectivity of the fully assembled units are tested in a setup at LSU using a LED
31 flasher. If LED light signals are seen the panel is successively immersed in gaseous
32 argon (GAr) along with an alpha source. The observation of argon scintillation light
33 originating from alpha particles and cosmic-rays penetrating the GAr volume allows

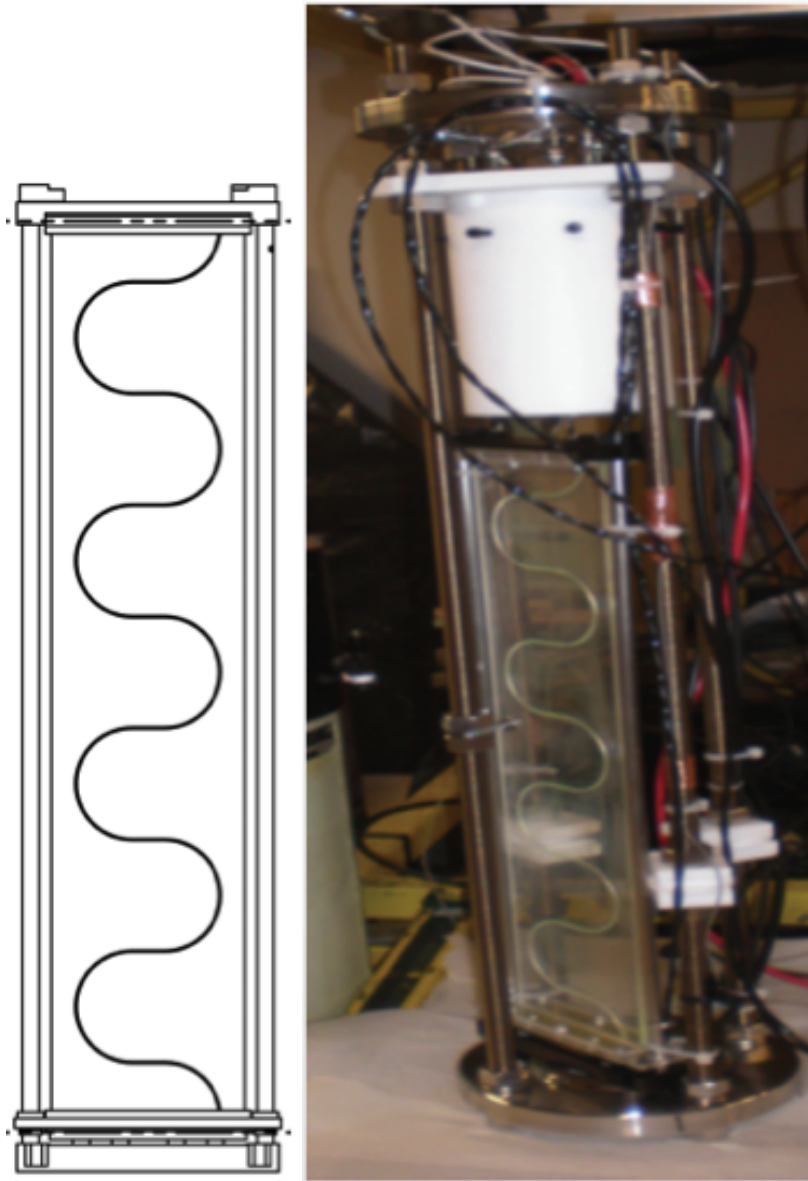


Figure 1.3: LSU photon-detection panel. Technical drawing of a $20'' \times 4.33''$ acrylic panel with embedded WLS fiber (left) and picture of a prototype in test set-up at LSU (right) with the same dimensions.

fig:1-LSU

34 for a relatively quick quality control check of a completed photon detector at room
35 temperature.

36 **1.3.4 Proof of concept and prototype detector results**

1 Several photon detector panels of $20'' \times 4.33''$ have been produced and two have been
2 tested in a LAr test stand at CSU. The detectors submitted to the cold test have
3 3 and 2 embedded fibers, respectively, but are otherwise produced in the same way.
4 The data taking in LAr included self triggered alpha source scans as well as cosmic
5 runs with a muon hodoscope providing a trigger for near vertical muons penetrating
6 the LAr volume.

7 **Alpha source runs:** The alpha source was placed at a distance of about 1" in
8 front of the center line of the photon panel and moved to 20 different positions
9 spaced about 1" apart from neighboring positions. At each position 5000 signal
10 traces were recorded and measurements were repeated for three of the positions to
11 check the reproducibility of the measured light yield. Figure T.4 shows results for
12 both successively measured panels. The red and blue dots show the mean light yield
13 values in units of p.e. (photo electron equivalents = no. of fired SiPM pixels) for the
14 SiPM on the top and bottom end of the panel as function of source position. Green
15 dots show the sum of both channels. The summed signals provide a very uniform
16 detector response for the entire panel and independent of the alpha source position.
17 The data also indicate good reproducibility for the doubly measured positions. The
18 3-fiber panel shows about 50% more light when compared to the 2-fiber panel which
19 is in good agreement with expectations. It needs to be pointed out that the LAr
20 purity was not monitored and that measurements for the two panels were performed
21 sequentially after refilling the dewar with LAr. However, the liquid argon for both
22 measurements came from the same batch which motivates the assumption that the
23 purity for both measurements was very similar.

24 **Cosmic trigger runs:** Two $1'' \times 10''$ wide scintillator counters were placed above
25 and below the dewar to form a muon hodoscope and to select near vertical muons
26 traversing the LAr volume. The 3-fiber LSU panel and one LBNL/Elgin Bis-MSB
27 doped polystyrene bar of LBNE baseline dimensions and read out by three SiPMs
28 were simultaneously inserted in the LAr. The setup allowed the study of the response
29 of these photon detectors to scintillation light created by penetrating cosmic muons.
30 A detailed quantitative comparison of the relative light yield was not possible with
31 this setup due to large systematic uncertainties in the position dependence of the

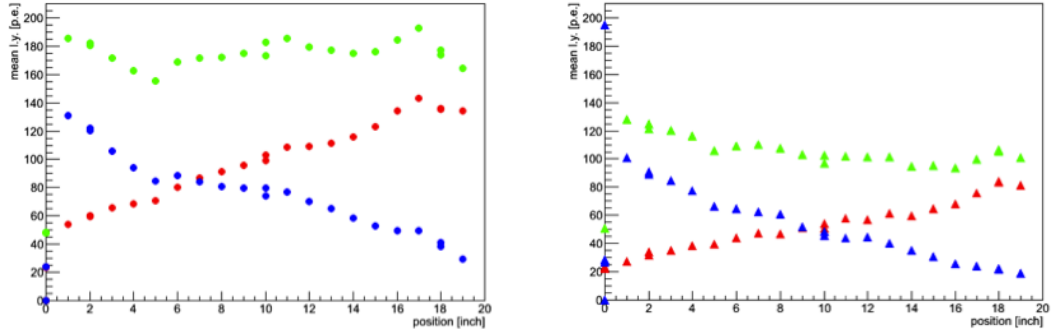


Figure 1.4: Light yield for the 3 (left) and 2 (right) fiber LSU photon detection panels in response to a 1" distant alpha source in LAr. Red and blue symbols represent the mean light yield over 5000 trigger events from a single SiPM each and green points represent the summed signal from both SiPMs.

fig:2-LSU

³² scintillation light generation by the triggering cosmic muons. A qualitative comparison
³³ of the detector responses, taken as the signal sum of 3 and 2 SiPMs for the
³⁴ Elgin bar and the LSU panel, respectively, shows comparable light yields as shown
¹ in figure 1.5.
^{fig:3-LSU}

² 1.3.5 R&D Work in progress and present Plans

³ After the construction and proof of principle test of the LSU style photon detection
⁴ panels we manufactured several 2.17m long and 110mm (=4.33") wide panels to
⁵ demonstrate the scalability of the design. At the time of writing tests in the large
⁶ LAr dewar at CSU are in progress. We are performing alpha source scans and
⁷ cosmic muon runs. The alpha source scan runs are arranged such that the source
⁸ illuminates two photon detectors at the same time. This setup facilitates quantitative
⁹ and relative light yield comparison between different photon detector designs in the
¹⁰ same LAr bath with a well defined VUV light source.

¹¹ Manufacturing and testing of wider panels is under consideration to maximize
¹² the photon detector panel area in the ELBNF LAr far detector. The goal is to cover
¹³ the entire anode plane assembly (APA) area with photon detectors embedded into
¹⁴ the APA frame. Another important measurement goal is to establish the energy
¹⁵ threshold of the photon detection panels. A study will be conducted for the photon
¹⁶ detectors presently installed in the 35t detector using Michel electrons. The 35t
¹⁷ detector contains one of the 3-fiber LSU photon detection panels. In addition, alpha

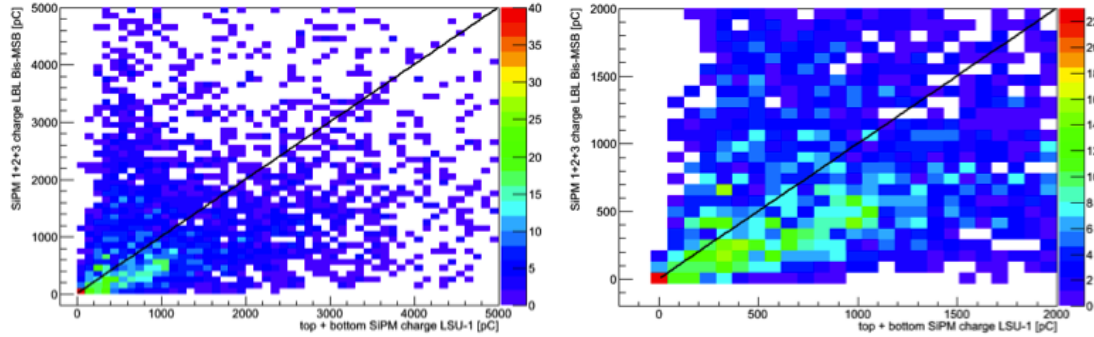


Figure 1.5: Scatter plot of the summed charge of 3 SiPMs coupled to the LBNL/Elgin Bis-MSB doped bar and the summed charge of 2 SiPMs for the 3-fiber LSU panel in response to an external muon hodoscope trigger. The right plot shows a zoomed version of the left plot.

fig:3-LSU

source runs in a well-controlled and monitored LAr setup may provide information on the particle energy threshold for observation of VUV scintillation light. The measurement of a photon detector panel's light yield as function of the source distance is another key measurement to estimate the response and sensitivity of the full photon detection system in a LAr detector. Results will be useful to validate MC simulations. We are exploring options to perform these tests in the large dewar setup at CSU or alternatively in the TallBo setup at FNAL.

The TPB coating procedure of the acrylic panels has not yet been optimized and improvements may be possible. We foresee a systematic study to identify parameters in the TPB dip and alternatively the evaporation coating procedure to maximize the light yield of resulting samples. These tests will be performed on small $10 \times 10 \text{ cm}^2$ acrylic panels with a U-shaped embedded WLS fiber. On the software and analysis side we are in the process of improving our tools to study position dependence for alpha source run data using relative signal timing and size. Furthermore, we plan to continue work on analysis algorithms to identify the late light component from argon scintillation.

Finally, early exploratory work on wallpapering the TPC cathode planes with TPB coated Tetratex foils and observing the shifted light with suitably installed photon sensors in combination with light collector cones will be pursued and explored more rigorously to provide timely results.

¹⁸ 1.3.6 Fiber bundle with WS-coated readiator

¹⁹ The driving cost of the photon detector system is readout electronics. A reduction in
²⁰ attenuation length has been observed for acrylic waveguides that have been doped with
¹ TPB. Once scenario to address this reduction is to populate the PD system with half-
² length paddles. Of course this leads to an increase in the number of readout channels.
³ While it may be possible to combine readout channels to mitigate the increase in
⁴ overall number a more desirable soultion would be to address the attenuaton length
⁵ issue.

⁶ To mitigate the reduced attenuation length of acrylic and polystyrene that have
⁷ been either doped with or coated with TPB the CSU group has been developing an
⁸ alternative design that is based on UV to blue wavelength shifting fiber (Y11) that
⁹ has not been treated with TPB. A thin TPB coated acrylic radiator located in front
¹⁰ of a close packed array of WLS fibers. Figure ¹¹ fig:fiber_bundle is a photograph of the fiber-bundle
¹¹ prototype.



Figure 1.6: Photograph of fiber-bundle PD prototype (early one-sided version). The thin
¹² TPB-coated radiator is mounted on top of the prototype in the image.

fig:fiber_bundle

¹² The VUV photons are incident on the TPB-coated plastic radiator and roughly
¹³ half of the photons converted in the radiator are incident on the bundle fiber bundle.
¹⁴ The photons in the Y11 fiber are then which are directed onto SiPMs at one end.

15 The Y11 fiber (from Kuraray) have mean absorption and emission wavelengths of
16 about 440 nm and 480 nm respectively. The attenuation length of the Y11 fibers
17 is given to be greater than 3.5 m at the mean emission wavelength, which allows
1 production of full-scale (2.2 m length) photon detector paddles.

2 First prototypes of this design utilized two rows of fibers with a reflecter behind
3 the doubled row to redirect the 400 nm photons back through the two rows if they
4 weren't absorbed on the first pass through. Based on data taken at the CSU Cryo-
5 genic Detector Development Facility (CDDF) and the Fall 2014 FNAL Tallbo test,
6 only a single row design could be considered - and is currently under development.
7 Data taken at both tests showed that the front row of fibers collected twice as much
8 light as the back row of fibers. The current design utilizes two single rows of fibers
9 back-to-back with layers of Tyvek diffuse reflector in between.

10 Another benefit of this design is that an arrangement with back-to-back rows of
11 fibers separated by an opaque reflector arranged would then face into different TPC
12 cells allowing additional information to be used in the disambiguation of the TPC
13 signals coming from wire wrapping on the APA frames. A further benefit of the
14 design could be compatibility with concepts where the walls of the detector are
15 covered with TPB coated material shifting the VUV photon to blue and then the
16 WS-fiber can capture the emitted light. Further study is required to determine the
17 effect of these enhancements on physics reach of the detector.

18 To fully exploit this approach several design optimizations need to be examined
19 including the following:

- 20 • TPB coating thickness on thin radiator
- 21 • Double-ended readout. If the fibers are readout out from both ends and the
22 corresponding channels are ganged onto one readout channel an increase in
23 channel output can be obtained without significant cost.
- 24 • Use of custom doped fibers to best match the QE response of the SiPMs and
25 the emission spectrum of the TPB.
- 26 • Remove the radiator and coat the TPB directly onto the outer fiber cladding
27 of the Y11 fibers. Since the fibers are double-clad it may be the case that the
28 attenuation length of the fibers is not altered by the TPB application. The
29 geometry of the close-packed fiber row may lead to increased photon (400 nm)
30 collection

31 The cost of this design is comparable to that of the bar-based design but is slightly
32 more complex to fabricate - although the Y11 fibers are commercially available which

33 is an attractive feature. The engineering aspects of the design will be discussed in
34 the appropriate section of this chapter.

35 **1.4 SiPM**

¹ **1.5 Mechanical Support**

2 Mechanically supporting the photon detector systems in the APA frames presented
3 several challenges, including the need to support three different light collecting and
4 wavelength shifting technologies in a package utilizing the same mounting features in
5 the APA frames, and the effects of varying thermal contraction of various materials
6 at 80 degrees Kelvin which complicated both light collector and SiPM mounting.

7 The baseline design for mounting the PDs into the APA frames calls for ten PD
8 modules, approximately 2.2m long, mounted roughly equally spaced along the full
9 length of the APA frame (Figure 1.7). The PD modules are read out using individual
10 twisted pair cable, one per SiPM. These cables (120 of them in the original baseline
11 design) are routed through the APA side tubes to a connector at the cold electronics
12 readout end of the APA. Initially it was decided that it would be too complicated
13 to design the APA frames to allow PD module installation following APA wire-
14 wrapping, so the PD modules were installed prior to this step in the installation
15 process. The Wavelength shifting elements in the light collectors of the PD modules
16 are sensitive to heat, humidity and most critically to exposure to ambient light,
17 which places significant requirements on the environment the APAs are assembled
18 and stored in this way, but initially it was decided this was the best option.

19 A universal PD frame assembly was devised to hold all three PD design variations
20 under consideration. Figure 1.8 shows an example of a short (400 mm long active
21 area) version of this frame manufactured for the 35t test, and Figure 1.9 shows a
22 mechanical assembly drawing of the frame system for one of the candidate light
23 collector choices. The frame consists of two plastic (acetal) end caps mounted to the
24 inside of the APA frame, joined by 10 mm diameter stainless steel tubes which run
25 the full width of the APA frame, providing intermediate support for the PD modules
26 as needed. The SiPM mount PCBs are incorporated into one of the end blocks,
27 along with the cable connections for the twisted pair cables. Due to the significant
28 variations in coefficient of thermal expansion between the stainless steel frame and
29 the plastic WLS elements, we expect a relative difference in thermal contraction of
30 1% at LAr temperatures. The far endblock assembly provides balancing forces to
31 the light collector elements as required to ensure these elements remain in straight

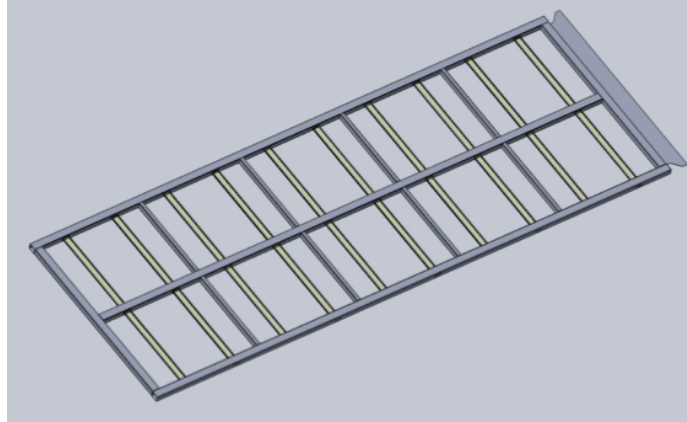


Figure 1.7: Full APA frame with ten photon detectors mounted inside the frame

fig:5.5-1

³² and in good contact with the SiPMs.

³³ Testing of the PD mount scheme in many test setups (at IU, CSU and FNAL),
³⁴ as well as experience APA assembly, have led to a re-evaluation of the PD mounting
¹ scheme. The revised baseline has PD installation occurring following ^{fig:3.5-4} APA wire
² wrapping, through slots left in the side of the APA frame (Figure 1.10). As shown
³ in the figure, the plan still calls for ten PDs per APA frame. Five of the PDs will
⁴ be installed through each side of the APA frame, and the cables for each of the
⁵ PDs will be routed to the cold electronics end of the APA inside the side tube the
⁶ PD was inserted through. Stainless steel c-channels mounted into the APA frames
⁷ prior to wire wrapping will guide and support the PDs during and after installation.
⁸ The PD will only be attached to the APA frame at one end, so the purely-plastic
⁹ PD module will be free to slide in the track to allow for the differential contraction
¹⁰ (^{fig:5.5-5} Figure 1.11). Tests of 2.2m prototype assemblies of both fiber hybrid and the
¹¹ LSU-proposed monolithic acrylic bar design in the CSU CDDF have demonstrated
¹² significant promise. This installation scheme

¹³ Thermal contraction at cryogenic temperatures also complicates the mounting
¹⁴ of the SiPMs in the PD modules. The baseline sensL SiPMs are surface mount
¹⁵ components, with 4 0.5 X 0.5mm pads for making electrical contact. Reliability and
¹⁶ elevated dark count rate problems, as well as physical delamination of the SiPM front
¹⁷ face from the silicone substrate, were observed early in cryogenic testing of SiPMs,
¹⁸ and suspicion fell on the mechanical contact between the mounting PCB and the
¹⁹ SiPM itself.

²⁰ Three different methods of making these electrical contacts: Soldering the SiPMs
²¹ directly to the PCBs (fig 5.5-6a), using commercial spring-loaded electrical contacts

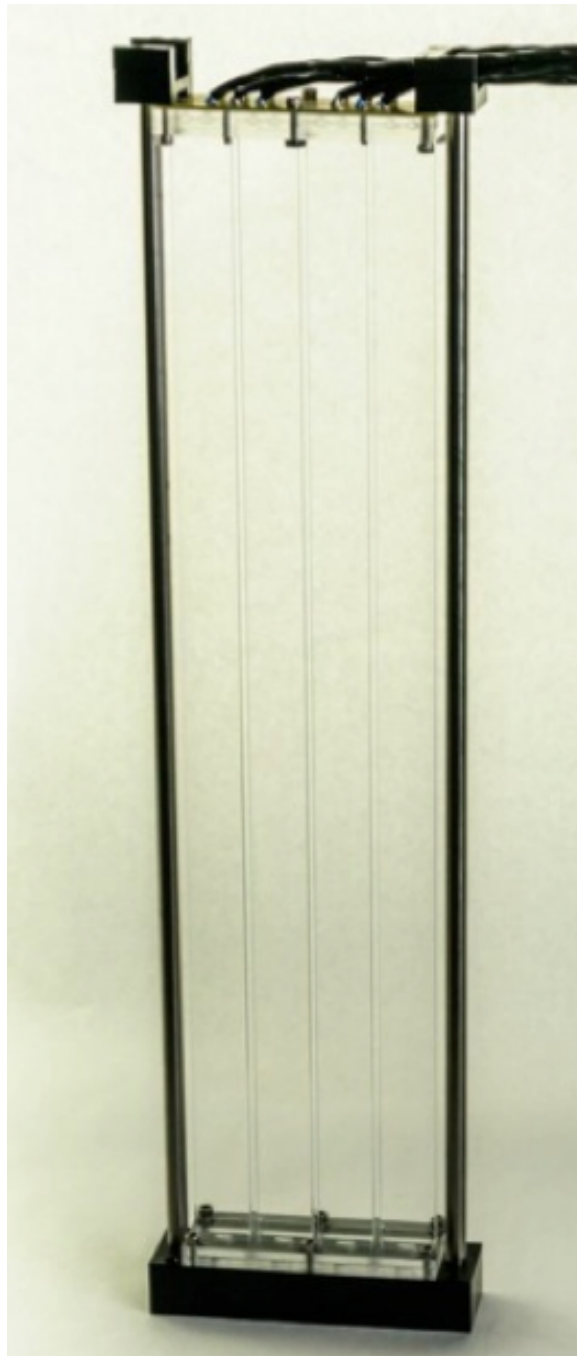


Figure 1.8: Photograph of 40 cm long bar-based prototype mounted in test frame

fig:5.5-2

Design for a Deep Underground Single-Phase LArTPC

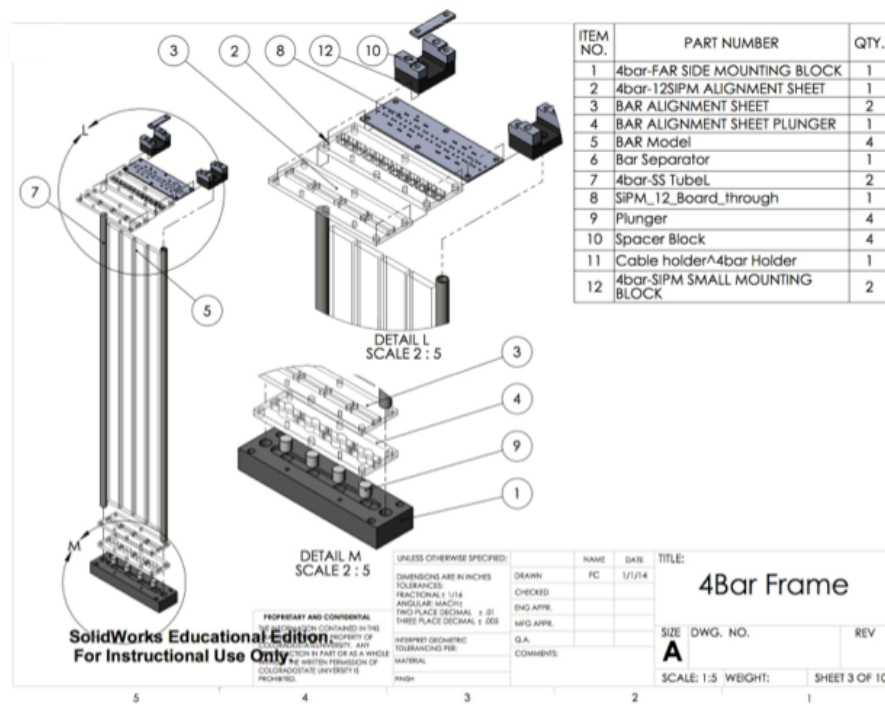


Figure 1.9: Mechanical assembly drawing of frame system

fig:5.5-3

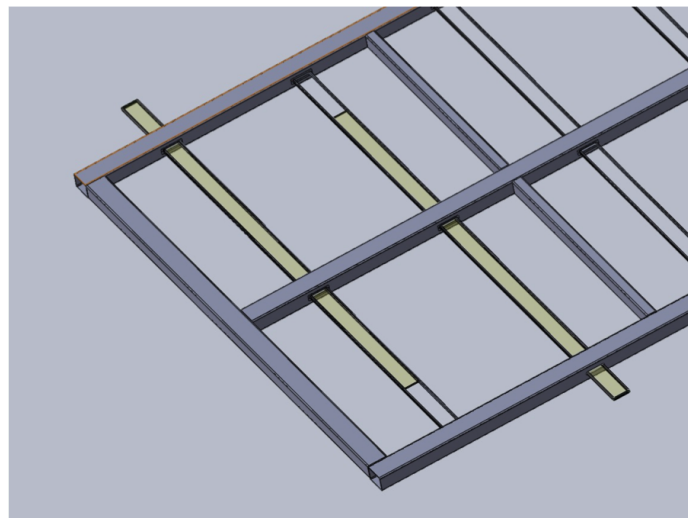


Figure 1.10: Blow up of APA fram showing PD insertion location

fig:5.5-4

Design for a Deep Underground Single-Phase LArTPC

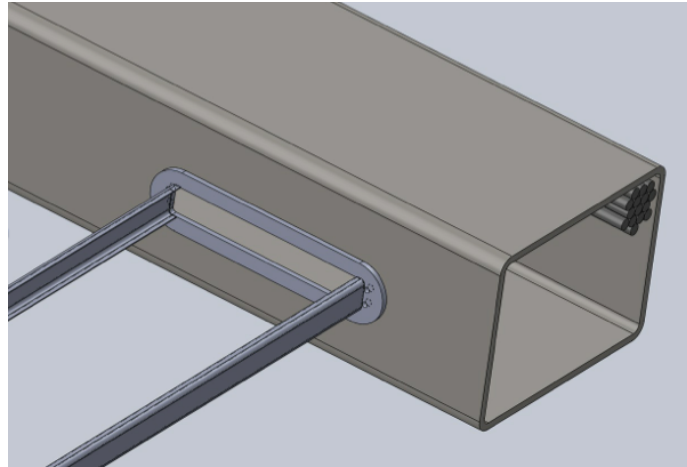


Figure 1.11: Slot and rail showing mounting location of photon detector

fig:5.5-5

²² or μ JIPogo pins^{fig:5.5-6b} (Figure ??),

²³ check ref

²⁴ and soldering short wires to the SiPM pads and thence to the PCB (Figure ??).^{fig:5.5-6c}

¹ check ref

² Each of these methods provides assembly challenges, and cryogenic testing has
³ not suggested a clear choice so far. Testing and development are still underway to
⁴ resolve this issue.

5 1.6 Photon System Readout Electronics

sec_elec

6 1.6.1 Reference Design

⁷ Scintillation light from LAr comes from the two different excited states with lifetimes
⁸ of about 6 ns and 1.6 μ s. Only a limited amount of light is collected by this system,
⁹ so the electronics must be designed to collect the light from both excited states. A
¹⁰ summary of the general requirements for the system, including requirements from a
¹¹ physics performance perspective, are given in Table 1.3.^{tab:reeq}

¹² The plans for the electronics for the photon detection subsystem include a baseline
¹³ design with several options that remain R&D activities. There alternative implemen-
¹⁴ tations of electronics are described in Section 1.6.2.^{sec alt}

¹⁵ In the baseline plan, there are no front-end electronics in the cold volume. In-
¹⁶ stead, the un-amplified signals from the SiPMs are transmitted to outside the cryo-

Table 1.3: Physics requirements for the photon detector electronics

Performance Parameter	Target
Time Resolution	Better than 30 nS wrt event time zero ("t0")
Charge Resolution	0.25% photo-electron equivalent
Dynamic Range	$\sim \times 10$ better than detector (1000:1)
Linearity	Sufficient to resolve 1 photo-electron signals
Multi-Hit Capability	Sufficient to measure Triplet (late) Photons
Dead Time	Live up to 2 drift times either side of beam spill
Bias Control	0.1 V resolution up to 30 V per channel
Calibration	On-board Charge Injection
Timing	Events time-stamped using NO ν A Timing syst.

17 stat on cables for processing and digitization, as shown in Figure 1.12. There are
 18 advantages and disadvantages to this approach. The advantages are that the infra-
 19 structure required for inside the cryostat is reduced (power, data cables, precision
 1 clocks, data protocols, etc.); reliability is improved (no single-point failures of multi-
 2 channel devices inside the cryostat); serviceability and accessibility to the front-end
 3 electronics are improved; and the need to develop cold electronics, possibly a custom
 4 ASIC, is eliminated. The disadvantages are that the cable plant inside the detec-
 5 tor is increased, which can create mechanical challenges and installation difficulties;
 6 the flange board (warm/cold interface) is more complex; there are generally more
 7 connectors in the system; and signal-to-noise considerations are more difficult. Gen-
 8 erally, the baseline design favors simplicity, reliability and reduced R&D time and
 9 costs, and also meets the performance requirements of the electronics.
 10

No fig1 exists for: Block diagram of the photon detector signal processing sys-
 tem.

Figure 1.12: Block diagram of the photon detector signal processing system

fig:fig-e-1

11 In the 35-ton prototype, each SiPM signal was transmitted on an individual
 12 shielded twisted-pair cable fitted with individual LEMO-style connectors. The bias
 13 voltage was coupled onto the signal cable, using AC-coupling on the receiving end to
 14 measure the SiPM signal. The use of high-quality cable with point-to-point connec-
 15 tions between an individual SiPM inside the cryostat and the front-end electronics
 16 residing outside the cryostat, combined with good differential signal processing on the

17 receiving end, enabled the demonstration of the principle that single photo-electron
18 signals could be measured accurately without the need for cold electronics. In order
19 to address the problems with the cable plant as identified above, the following ideas
1 are being pursued:

- 2 ● Ganging together of several SiPM outputs from a given PD detector into one
3 output cable. This increases the detector capacitance, affects the pulse shape,
4 and could spoil the timing resolution of the measurement. Also, the SiPMs
5 may have to be preselected, since there will be only one bias voltage for three
6 devices, and it may be important to match the over-voltage characteristics.
7 Studies are in progress to find a compromise between data precision and cabling
8 issues. One approach is to add a cold pre-amplifier if the ganging together of
9 several SiPMs result in performance that is too degraded to meet specifications.
10 The infrastructure requirements (cables, connectors, power, cold performance,
11 reliability, mechanical mounting, etc.) would have to be considered.
- 12 ● Use of multi-conductor, individually shielded pair cable. A candidate cable
13 containing four individually-shielded twisted pairs has been identified and tests
14 are in progress. The cable is in Teflon jacket, which should be acceptable for
15 use in LAr.
- 16 ● Use of mass-terminated connectors. Several candidate connectors for use with
17 the cable described above are being pursued.

18 The baseline plan assumes that three SiPM signals can be ganged together into
19 one readout channel. By using the multi-conductor cable with four twisted pairs,
20 this results in one cable per PD consisting of 12 SiPMs. The diameter of this cable
21 is xxx mm, which reduces the cable plant by $\sim x10$ compared to that used in the
22 35 ton detector. The cost of the connectors also decreases by $\sim x10$. Lastly, the
23 ease in making connections at the flange board will be improved by the use of a
24 mass-terminated connector.

25 In the baseline plan, the front-end electronics resides outside of the cryostat in
26 instrumentation racks. We have designed and built a custom module for receiving
27 SiPM signals, and performing signal processing in the front-end as preprocessing for
28 trigger and DAQ. The module is called the SiPM Signal Processor (SSP). An SSP
29 consists of 12 readout channels packaged in a self-contained 1U module. Each channel
30 contains a fully-differential voltage amplifier and a 14-bit, 150 MSPS analog-to-digital
31 converter (ADC) that digitizes the waveforms received from the SiPMs. The front-
32 end amplifier is configured as fully-differential with high common-mode rejection, and
33 receives the SiPM signals into a termination resistor that matches the characteristic

34 impedance of the signal cable. Currently there is no shaping of the signal, since
35 the SiPM response is slow enough relative to the speed of the digitization to obtain
36 several digitized samples of the leading edge of the pulse for the determination of
1 signal timing.

2 The digitized data is stored in pipelines in the SSP, for up to $\sim 13 \mu\text{s}$. The
3 processing is pipelined, and performed by a Xilinx Artix-7 Field-Programmable Gate
4 Array (FPGA). The FPGA implements an independent Data Processor (DP) for
5 each channel. The processing incorporates a leading edge discriminator for detecting
6 events and a constant fraction discriminator (CFD) for sub clock timing resolution.
7 Because the FPGA is programmable and accessible, it is possible to explore different
8 data processing algorithms and techniques, and even customize the readout for a
9 given type of event (supernova for example.) A picture of the module is shown in
10 Figure 1.13. A block diagram of the system is shown in Figure 1.14.

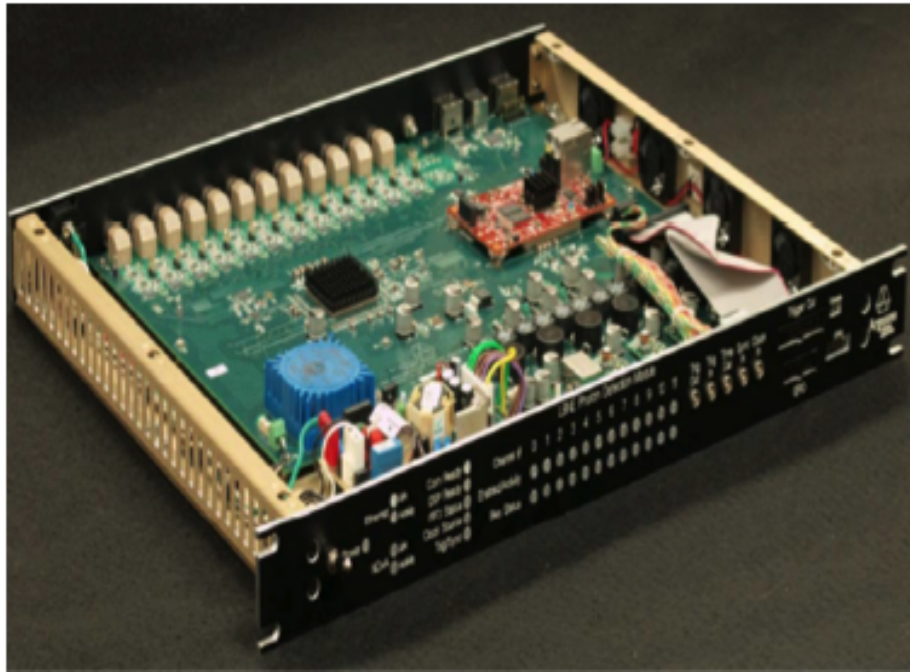


Figure 1.13: Picture of the SSP module

fig:fig-e-2

11 In the simplest mode of operation, the module can perform waveform capture,
12 using either an internal trigger or an external trigger. Up to 2046 waveform samples
13 may be read out for each event. When waveform readouts overlap the device can
14 be configured to offset, truncate or completely suppress the overlapping waveform.

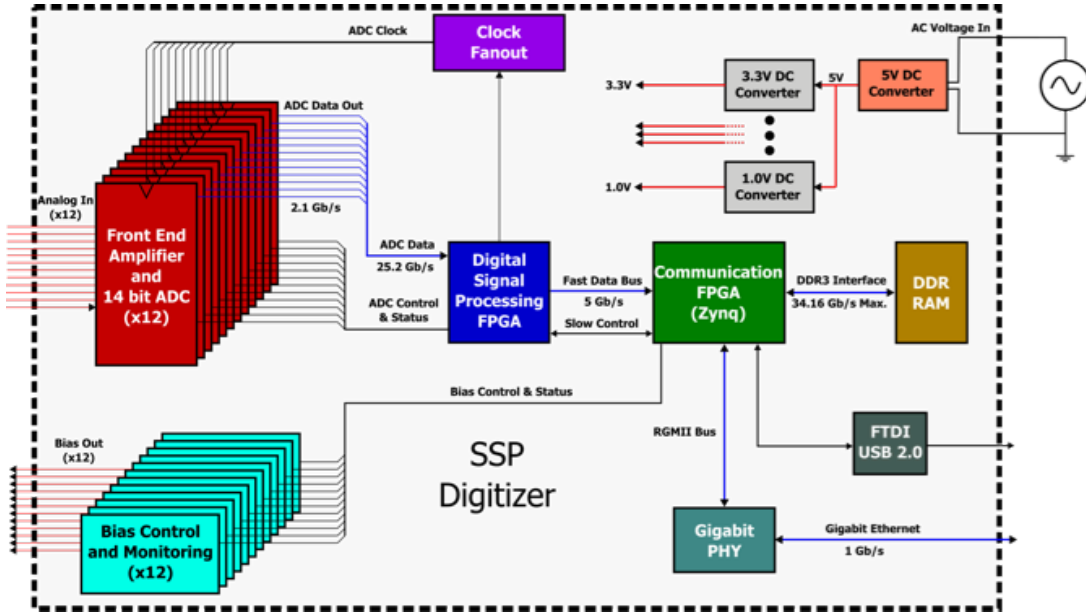


Figure 1.14: Block diagram the SSP module

fig:fig-e-3

¹⁵ Pile-up events can also be suppressed.

¹⁶ As an alternative to reading full waveforms, the DP can be configured to perform a wide variety of data processing algorithms, including several techniques for measuring amplitude, and also timing of the event with respect to a reference clock. All timing and amplitude values are reported in a compact event record. Each data processing channel stores up to 340 event records when not storing waveforms.

⁴ Generally, the SSP performs pipelined processing. The module has been designed to support several different triggering schemes, including self-triggered, use of an external trigger, or use an external gate to readout all events within a time-window. In order for the events measured in the photon detector to be matched up with the corresponding events in the TPC, the front-end electronics attaches a timestamp to the data as it is acquired. The timestamp is unique, and has a correspondence with the timestamps in the TPC electronics processing. The timestamp in the SSP is applied to the event data as it is digitized, and becomes part of the data as the processing proceeds. In the case where zero-suppression and data sparsification are used, the timestamp on accepted data remains intact. To achieve this, the TPC and PD electronics must be synchronized, including timestamp counter resets, and a known and stable calibration between the corresponding timing resolution of the ADC conversion in the two systems. The electronics has been designed to support

¹⁷ a full interface to the NO ν A timing system, which is the baseline timing system for
¹⁸ the experimental prototypes.

¹⁹ A Xilinx Zynq FPGA, onboard the MicroZed system-on-module, handles the slow
¹ control and event data transfer. The SSP has two parallel communication interfaces;
² USB 2.0 and 10/100/1000 Ethernet. The 1 Gb/s Ethernet supports full TCP/IP
³ protocol. The module includes a separate 12-bit high-voltage DAC for each channel
⁴ to provide up to 30 V of bias to each SiPM. The module also feature charge injection
⁵ for performing diagnostics and linearity monitoring, and also voltage monitoring.

⁶ In tests to date, the SSP is capable of measuring single photo-electron signals
⁷ coming from the SiPMs over a cable length of 30 meters when the SiPMs are operated
⁸ at LAr temperatures. The timing resolution of the signals has been measured to be
⁹ better than 3 ns. The full-differential signal processing in the front-end circuitry is
¹⁰ important in achieving this result.

¹¹ The SSP is self-contained in that it receives 60 Hz, 120V power, and has internal
¹² linear and DC/DC power supplies for generating the DC voltages needed for the
¹³ instrumentation, as well as the bias voltage for the SiPMs. The SSP is packaged in
¹⁴ a 1U, rack-mountable package. For the 35-ton prototype, the racks are located near
¹⁵ the ports on the top of the cryostat.

¹⁶ 1.6.2 Alternatives

¹⁷ sec_alt In the baseline design of the PD electronics, the approach was taken to have no
¹⁸ electronics inside of the cold volume. This results in a large number of cables and
¹⁹ connectors. Other experiments using liquid argon have successfully implemented
²⁰ cold TPC electronics, thereby significantly reducing the cable plant that must come
²¹ through the cryostat.

²² This approach has challenges in power distribution, heat dissipation, and the
²³ performance of front-end electronics in LAr. To address serviceability, the cold elec-
²⁴ tronics might be realized in a modular way and situated just below the flange in
²⁵ the cryostat so that it can be accessed in the event that repair is needed. To this
²⁶ end the zero-suppression will be important to avoid high data rates depending on
²⁷ the number of readout channels needed. A way to realize the cold zero-suppression
²⁸ would be to implement a cold FPGA (or an ASIC, yet to be developed). So far the
²⁹ cold FPGAs have had mixed results in tests.

³⁰ An alternative approach would be to perform an “analog zero suppression” with a
³¹ constant-fraction discriminator and then gate the signal and digitize warm, in which
³² case the complication with encoding the particular channel has to be addressed.
³³ The significant challenges in this technique include power dissipation, the increased

34 possibility of contamination of the LAr, and extended infrastructure requirements
35 that must reside in the cold volume. The virtue is that this can significantly reduce
36 the number of signal penetrations into the cold volume.

1 The electronics for the photon detector of LBNE uses fast (direct) digitization of
2 the SiPM pulses. Another option for the front-end electronics is to use pulse shaping.
3 Instead of digitizing the full bandwidth of the SiPM signal, the pulse is shaped using
4 analog filtering techniques, generally producing a pulse with a prescribed shape with
5 a peak that is proportional to the total amount of charge. By measuring the peak,
6 both amplitude and pulse timing can be obtained. Since the pulse response follows
7 a known transfer function, the pulse peak can be obtained using slower synchronous
8 sampling, or using asynchronous sampling through the use of peak detection and
9 constant fraction discrimination.

10 In either case, the data can be processed by an FPGA using algorithms optimized
11 for the application. In particular, assuming that a sufficient number of samples are
12 obtained of the shaped pulse, a chi-square comparison of the shape to the ideal
13 pulse can be used to determine pulse corruption, or event identification. As with
14 direct digitization, the digitization clock and timestamp can be synchronized using
15 an external clock source. The data can be read out in a similar manner, using USB
16 2.0 or 10/100/1000 Ethernet. The virtue of this approach is that a slower ADC can
17 be used, reducing power consumption, and also reducing data load and the speed
18 of readout links. The technique does trade bandwidth for shaping, making timing
19 and pile-up issues more important. This can result in the interpretation of the pulse
20 shape becoming more complex than direct digitization. Generally, the pulse shaping
21 circuitry is also less expensive than the direct digitization technique, assuming similar
22 performance requirements.

23 Another option for the photon system readout would include the use of an Application
24 Specific Integrated circuit (ASIC) as a way to reduce cost. The large channel
25 count in a real detector system is such that the production cost of the system could
26 be greatly reduced. Often, the cost of development of an ASIC from scratch is
27 quite high, of order \sim 400K, and can take \sim 1 to 2 years for development, so cost
28 and schedule must be weighed carefully. However, other benefits from the ASIC
29 approach include reduced space requirements for circuitry on the front-end, lower
30 power dissipation, and specialized functionality in the front-end chip.

31 There exist several ASICs that have been designed over the last few years especially
32 for SiPM readout. One could potentially explore the functionality and performance
33 of these designs, and evaluate their suitability for LBNE. This option might
34 be used either for warm or cold electronics. Direct digitization has the virtue of being
35 straight-forward from a circuit design perspective. By taking advantage of modern

36 high-bandwidth OP amps, high-speed, high-rate ADCs, and powerful FPGAs with
37 high-speed serial links, it is possible to obtain 14-bit dynamic range digitization with
38 ~ 1 ns timing resolution. By reading all of the samples into an FPGA having a deep
1 buffer, digital signal processing techniques can be employed using the programmable
2 logic, offering powerful analysis algorithms that can be developed in time. The tech-
3 nique generally has higher power consumption and tends to be more expensive than
4 simpler instrumentation techniques.

5 **1.7 Photon Detector Calibration**

6 sec_pd_calib
The photon detector calibration is a part of a larger calibration plan that covers all
7 aspects of an LAr detector calibration, and includes methods to convert collected
8 charge to initial particle's energy, as well as calibration techniques to convert col-
9 lected scintillation light into estimate of particle's interaction time, energy, and a
10 track/vertex location for each event.

11 As already described, the baseline for the scintillation photon detectors assumes
12 employment of acrylic light collection paddles to reduce the required costly photo-
13 cathode area. Several photon detector designs are presently being developed and are
14 being tested in small dewars. Since each of these new elements has not yet been
15 tested in a large-scale TPC, the 35-ton LArTPC prototype is being constructed to
16 provide essential design validation.

17 The current FD designs are anticipated to have sufficient sensitivity to provide
18 event timing information for atmospheric neutrino and proton decay channels. How-
19 ever, it will not provide high efficiency down to the 5-MeV neutrino energy level
20 desired by the supernova program. This would have the impact that the event re-
21 construction energy resolution would be 20% rather than 5% achievable with the
22 event time determination from a photon detector able to operate efficiently at a suf-
23 ficiently low energy threshold. The improvement in physics will be studied in the
24 near future but a substantial effort in development of improved detection techniques
25 is desired.

26 In the absence of precise physics requirements for the photon detector system
27 and in order to support R&D activities on the photon detector development it was
28 decided that the photon detector should provide a time stamp to determine the time
29 of occurrence of an event (so called "time zero") with an accuracy much better than
30 1 s

31 fix

32 .

33 Items relevant to the photon detector calibration are the fast and slow components
34 of the light, photon propagation including scattering and reflections, impact of N2,
35 E-field strength, as well as the energy range of interest. A calibration system that
1 addresses the issues listed above has to be both comprehensive and cost-effective,
2 and has to be tied to the overall calibration system that includes both charge and
3 scintillation light calibration techniques. Such a system will be designed in the future.

4 To support the PD R&D phase we designed a light-flasher based calibration
5 system that will serve to monitor the relative performance and time resolution of the
6 system. In particular, for anticipated 35-ton performance tests we need to evaluate
7 relative efficiencies of multiple light collection techniques in order to be able to down-
8 select an optimal light readout technology. The system that meets these requirements
9 will consist of a set of LEDs as light sources or a laser with a VUV wave-length,
10 coupled to quartz fibers, thus transmitting light from outside the detector volume
11 to desired locations at the CPA within a TPC. Therefore we will equip the 35-ton
12 detector with LEDs located and fired externally, with fibers running into the cryostat,
13 to diffusers that will emit light from the CPA to the APA.

14 For the 35-ton cryostat at the surface at Fermilab it will be complementary
15 to cosmic ray muon tracks as means of calibration. In terms of light sources the
16 measurements should be performed with an UV (245-375nm) light source. The UV
17 light mimics physics starting from the wavelength shifter conversion, light guide
18 propagation, photo-sensor detection and FEE readout. The external light-flasher
19 calibration system is designed under following assumptions:

- 20 • simple to implement (no active components within PD/APA, such as LEDs or
21 fibers mounted within APA).
- 22 • less-intrusive (less material within detector in terms of fibers, then equipping
23 each PD frame with individual fiber).?
- 24 • provide a benchmark light-based reconstruction with the use of localized light
25 sources distributed throughout the detector volume.
- 26 • has a potential to be adapted for deployment in a large Far Detector in the
27 future

28 We describe the system in Figure [fig:fig-c-1](#). The system consists of a 1U rack
29 mount Photon Detector Calibration Module (PDCM) sitting outside the liquid argon
30 cryostat. The module generates light pulses that propagate through a quartz fiber-
31 optic cable to diffusers at cathode-plane (CPA) to distribute the light uniformly
32 across the photon detectors mounted within anode plane (APA). There are 5 diffusers

- 33 on the CPA plane: one in the center and four diffusers close to the CPA corners, as
 34 shown in Figure 1.16.

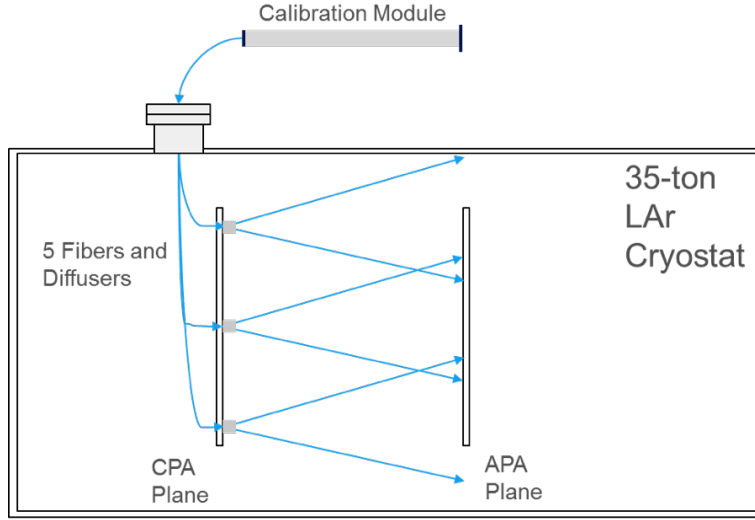


Figure 1.15: Concept of the UV-light calibration system for the photon detector in liquid argon

fig:fig-c-1

35 The PDCM module layout is shown in Figure 1.17. The ANL photon calibration
 1 module is based on a re-purposed SSP unit. An SSP board will be repackaged into a
 2 deeper rack mount chassis that will accommodate a new internal LED Pulser Module
 3 (LPM) and an additional bulk power supply. The LPM utilizes five digital outputs
 4 to control the LPM pulse and its duration (arrows in black). These LVDS outputs
 5 are derived from the charge injection control logic within the SSP's FPGA. The
 6 even channel SiPM bias DACs are repurposed to control the LPM pulse amplitude
 7 (arrows in red). The adjacent odd channels are used to readout a photodiode which
 8 is used for pulse-by-pulse monitoring of the LED light output. The output of the
 9 monitoring diode is used to normalize the response of the SiPMs in the detector to
 10 the calibration pulse

11 For the 280 nm light we have performed a simulation of the designed diffuse
 12 light calibration system using TracePro, a generalized 3-D light ray-tracing program
 13 with the ability to include bulk optical properties such as absorption, fluorescence,
 14 birefringence in addition to surface properties such as scattering and reflection. Fig-
 15 ure 1.18 shows simulated light distributions at the 35-ton APA for the cases of
 16 the VUV light emitted by either the central diffuser only (left figure), or by outer
 17 four diffusers simultaneously (right figure). A full Geant4 based simulation of the

fig:fig-c-3

fig:fig-c-4

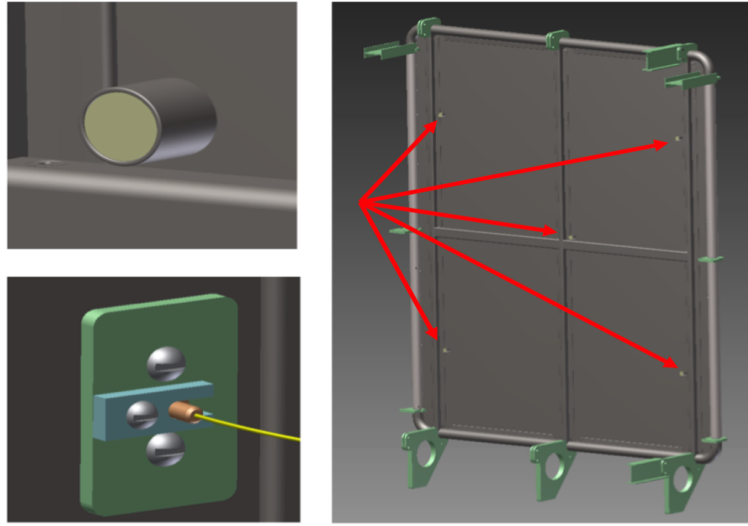


Figure 1.16: The diffuse light is emitted from diffusers (top left figure) mounted at five CPA locations, indicated by arrows (right figure). The UV light from the PDCM to diffusers is transported through quartz fiber (lower left figure).

fig:fig-c-2

18 detector will be used in the future. Using the preliminary data with the 35-ton style
 19 light guides (indicating 0.5% efficiency for number of photo-electrons per incident
 20 128 nm LAr scintillation photon 50 cm from the light guide), we estimate for 280
 1 nm light to observe 15 photo-electrons per single SiPM channel when the light is
 2 emitted from the single central diffuser in 13 ns long pulses. Similarly, we expect
 3 about 100 photo-electrons observed by a single SiPM channel when 280 nm light is
 4 emitted in 100 ns long pulses from the four outer diffusers at once.

5 In the LBNE prototypes (i.e. in 35-ton) and in Future Far Detector it will be im-
 6 portant to check if photon-detector components are functioning properly at various
 7 stages of the detector operation. Periodic light source deployments will monitor the
 8 systems stability as a function of time. A change in relative difference of UV light
 9 responses will indicate towards potential wave-length shifter instability, changes in
 10 SiPM gain and collection efficiencies. Much of the same monitoring is expected to be
 11 doable with cosmic rays in the 35-ton (at surface), with periodic LED/laser calibra-
 12 tion runs complemented with cosmic-ray data tracked with an external hodoscope.
 13 With the 35-ton detector one could use a well-defined muon trajectory defined by the
 14 hodoscope geometry and monitor the number of PEs per MeV of deposited charge.
 15 The number of PEs per PD channel from the well-defined muon track could be used
 16 as a calibration constant. However, for the deep underground LBNE the cosmic ray

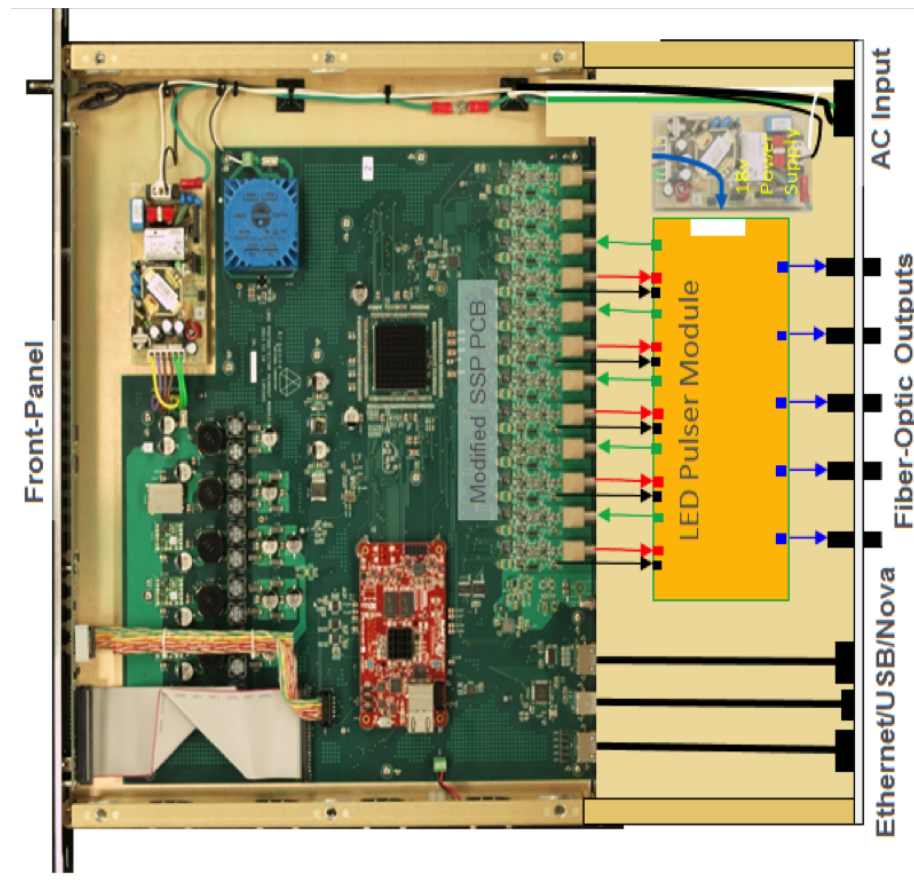


Figure 1.17: Photon detector calibration module (PDCM) layout

fig:fig-c-3

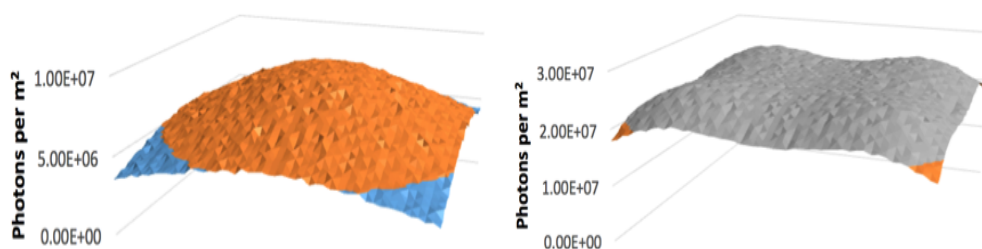


Figure 1.18: Simulated light distributions of the 35-ton APA for the cases of the VUV light emitted by either the central diffuser only (left), or by outer four diffusers simultaneously (right).

fig:fig-c-4

¹⁷ flux may inadequate for timely monitoring of the photon detectors. With the 35-ton
¹⁸ detector we have planned two sets of calibration runs:

- ¹⁹ 1. Calibration runs with four outer diffusers run simultaneously, in order to
 - ¹ -measure response of PD channels in multi-PE range and get integrated number
 - ² of event samples for each channel (for maximum light output)
 - ³ -test of the dynamic range from 1PE to maximum number of PEs.
 - ⁴ -repeat runs periodically to trace any changes in channel response.
- ⁵ 2. Runs with central diffuser only, in order to
 - ⁶ -perform initial calibration runs that will reveal malfunctioning channels, if
 - ⁷ any.
 - ⁸ -timing measurements with the 10-50 ns pulses, verify time resolution of the
 - ⁹ PD system.

¹⁰ The controlled source of light described here will be used to perform a relative
¹¹ ?t0? calibration, where the ?t0? could be absolutely calibrated with the use of the
¹² cosmic ray triggers available with 35-ton detector. Effects that contribute to a finite
¹³ time resolution and relative time offset of PD channels include scintillation time
¹⁴ constants, photon conversion with wave-length shifter, photon propagation through
¹⁵ PD paddle, SiPM jitter, and FEE resolution. Most these effects are constant and
¹⁶ can be individually measured on the bench, so the LED flasher system will monitor
¹⁷ overall stability of the photon detector. To go beyond the current R&D phase one
¹⁸ needs detailed MC simulations of light production, propagation, and detection to
¹⁹ perform comparisons of reconstruction performance against prototype data in terms
²⁰ of calorimetric energy and position reconstructions for measured event tracks. Future
²¹ light collection systems will aim to maximize the active area of the light guide bars, to
²² achieve a high photon detection efficiency with an optimized timing and granularity
²³ required for improved position resolution. As in the case with the TPC charge
²⁴ calibration we will need to evaluate what may be achieved with expected cosmic ray
²⁵ muons and Michels, π^0 , and natural radioactivity events (such as ^{39}Ar with end-point
²⁶ energy of about 500 keV).

²⁷ 1.8 Installation

²⁸ Installation of the photon detectors is one of the most significant factors driving the
²⁹ mechanical design. As discussed above, our initial thought was to install the PDs
³⁰ and run the SiPM twisted pair cable down the frame side tube prior to wire-wrapping
³¹ the APA. Following our experience with the environmental controls (primarily UV

32 filtered light) required by the PDs, as well as the difficulties in dealing with the
33 PD readout cable ends during wire-wrapping, it was decided to change the baseline
34 to include inserting the PDs following wire wrapping. In addition to relaxing the
1 physical constraints on the wire wrapping, this also relaxes a schedule connection
2 between the APA and PD fabrication. It is not necessary to install the PDs into the
3 APA frames until shortly prior to installation of the APAs into the cryostat.

4 As noted above, and shown in Figure 1.10, a total of 10 PDs are installed into
5 each APA frame, with 5 coming in from each side. The installation will occur with
6 the fully-assembled APA frame lying flat on an insertion station table. Prior to
7 installation, the PD cable bundle will be inserted into the APA side tubes. The
8 cable bundle will be pre-assembled prior to installation such that the end of each
9 cable will terminate at the correct slot for the PD to be connected. Our baseline
10 cable design has also been modified to a single cable with 4 individual twisted pairs
11 in a single jacket, so each APA side tube will only require 15 cables (3 per PD, 30
12 per APA). These cables extend approximately 30cm past the end of the APA tubes
13 at the cold electronics end of the APA, and following installation of the APA into
14 the cryostat are connected to long-haul cables for the run to the readout electronics
15 (see Figure ??- cable diagram). Needs to be made)

16 Following this step, 5 PDs will be inserted into the APA through one side frame,
17 with connections being made between the twisted pair cables and the SiPM PCB
18 just as the readout end of the detector enters the tube (See Figure ??). The PD
19 is then inserted the last 10cm into the frame, and affixed to the inner surface of
20 the APA tube (See Figure ??). The process is then completed for the 5 PDs to be
21 inserted from the opposite side.

22 Following insertion of the PDs, the environmental controls required for the PD
23 WLS materials (UV filtering, temperature and humidity control) will need to be
24 observed for the entire APA.